PCCP

PAPER

View Article Online
View Journal | View Issue

Cite this: *Phys. Chem. Chem. Phys.*, 2014, **16**, 9294

Reactive simulations of the activation barrier to dissolution of amorphous silica in water

Michael Kagan, Glenn K. Lockwood and Stephen H. Garofalini*

Received 3rd January 2014,
Accepted 30th March 2014

DOI: 10.1039/c4cp00030g

www.rsc.org/pccp

Molecular dynamics simulations employing reactive potentials were used to determine the activation barriers to the dissolution of the amorphous SiO_2 surface in the presence of a 2 nm overlayer of water. The potential of mean force calculations of the reactions of water molecules with 15 different starting Q4 sites (Q*i* is the Si site with *i* bridging oxygen neighbors) to eventually form the dissolved Q0 site were used to obtain the barriers. Activation barriers for each step in the dissolution process, from the Q4 to Q3 to Q2 to Q1 to Q0 were obtained. Relaxation runs between each reaction step enabled redistribution of the water above the surface in response to the new Q*i* site configuration. The rate-limiting step observed in the simulations was in both the Q32 reaction (a Q3 site changing to a Q2 site) and the Q21 reaction, each with an average barrier of $\sim$14.1 kcal mol^{-1}. However, the barrier for the overall reaction from the Q4 site to a Q0 site, averaged over the maximum barrier for each of the 15 samples, was 15.1 kcal mol^{-1}. This result is within the lower end of the experimental data, which varies from 14–24 kcal mol^{-1}, while *ab initio* calculations using small cluster models obtain values that vary from 18–39 kcal mol^{-1}. Constraints between the oxygen bridges from the Si site and the connecting silica structure, the presence of pre-reaction strained siloxane bonds, and the location of the reacting Si site within slight concave surface contours all affected the overall activation barriers.

I. Introduction

The dissolution mechanism for hydrated silicate glasses or crystals has been extensively studied over the past several decades using a variety of experimental and computational methods.[1–11] A better understanding of the process by which silicate glasses dissolve can have implications for the development of materials for nuclear waste storage, microelectronics, fiber optics, and management of fracture mechanics. It has been established that the crack tip velocity for amorphous silica is substantially higher in the presence of H_2O than it would be otherwise.[12–19] The lifetime stability and amount of radionuclides released by nuclear waste glass can vary considerably depending on the parameters for the dissolution mechanism. The rate expression and activation barrier for dissolution in water is affected by several conditions: pH, temperature, composition, and population of surface sites.[6,7,9,20–28] Prior computational work[5,7,20,29–32] at various conditions has yielded results that differ from experimental data for the activation barrier for dissolution quoted by Icenhower and Dove and the references therein.[33]

The dry amorphous silica (a-SiO_2) surface can be populated with four types of Si sites that are determined by the coordination number of the Si atom in question. The Si site can thus have between one and four Si–O–Si bridges (siloxanes), with each type of site traditionally classified by the number of attached oxygen that are attached to a second silicon: Q1, Q2, Q3, and Q4. The dissolution of silica occurs when a silicic acid ($Si(OH)_4$) molecule escapes from the surface, producing a Q0 site in solution. Dissolution can have four steps from the Q4 site to the Q0, each with an activation energy that will break one of the Si–O–Si bridges and convert the site by decreasing the bridging oxygen coordination number.

A variety of experimental data indicates that the activation energy for the dissolution reaction of silica should be in the range of 16–22 kcal mol^{-1}, as reported by Pelmenschikov *et al.*[5] or 14–24 kcal mol^{-1} as reported by Wallace *et al.*,[30] or $\sim$14–20 kcal mol^{-1} from Icenhower and Dove.[33] The dissolution reaction is given as:

$$\text{Si–O–Si} + H_2O \rightarrow \text{Si–OH} + \text{HO–Si} \quad (1)$$

Ab initio molecular orbital calculations performed by Xiao and Lasaga showed that the pH affects the activation energy by changing the reaction catalyst.[20] The alkali range produced a barrier of 18.9 kcal mol^{-1} when the catalyst was OH^- and the acidic range produced a barrier of 24 kcal mol^{-1} when the catalyst was in H_3O^+. Hydrolysis of the siloxane bond by H_2O required considerably more energy at 29 kcal mol^{-1}. Similar *ab initio*

Interfacial Molecular Science Laboratory, Department of Materials Science and Engineering, Rutgers University, Piscataway, NJ, 08854, USA.
E-mail: shg@rutgers.edu

results by Pelmenschikov *et al.* using cluster models designed to show the role of the connecting lattice on restricting relaxations by fixing the positions of the border atoms in the clusters led to activation energies for Q1, Q2, and Q3 rupture of the Si–O–Si bridge of 29, 33, 49 kcal mol^{-1},[34] all higher than the unrestricted cluster case. Additional results by Pelmenschikov *et al.* on the Q2 and Q1 species of a quartz–water interface with a pH of 3, corresponding to the point of zero net proton charge[5] showed the energy barrier for the dissolution of the Q1 and Q2 siloxanes to be 20 and 29 kcal mol^{-1}, respectively. The higher barrier for Q2 was attributed to the fact that the Q1 site did not experience lattice resistance of the Q2 site. *Ab initio* calculations by Wallace *et al.* showed an activation energy of 38.7 kcal mol^{-1} for a Q3 siloxane in a cluster derived from quartz and H_2O,[30] which is higher than the range of experimentally obtained barriers (14.3–23.9 kcal mol^{-1}) that they cite. Quartz and a-SiO_2 are chemically equivalent but are thought to have different activation energies at an interface with water due to the different population of sites at the surface.[35]

Walsh *et al.* also used *ab initio* calculations to model the hydrolysis of a-SiO_2 surfaces and calculate the barrier for a dissociation of a siloxane bridge.[31] The barriers for comparable defect sites and surface ring structures constrained by cluster geometry were about 24 kcal mol^{-1} when one H_2O molecule was used. The authors suggested that the barrier for dissociation of the bridge could potentially be lowered by the cooperative hydrolysis of surrounding H_2O molecules serving to mediate ionic catalysis of the site. Del Bene *et al.* used *ab initio* quantum mechanical calculations to show that the barrier was affected by the presence of more than one H_2O.[32] A barrier of 30 kcal mol^{-1} was reported there for siloxane dissociation of a-SiO_2 in the presence of a water dimer. The authors noted that a complex rearrangement of protons at the site bridge leading to dissociation could be accomplished most easily by the concerted action of several H_2O. *Ab initio* calculations by Criscenti *et al.* have produced results showing an activation energy of 28.7 kcal mol^{-1} for an a-SiO_2 Q3 site and 17.7 kcal mol^{-1} for a Q2 site.[7] The authors used a cluster model with four H_2O molecules and one H_3O to suggest that the rate limiting step in a-SiO_2 dissolution was the breaking of siloxanes in either Q2 or the Q1 sites. The activation barriers determined by the computational methods of both Criscenti *et al.* and Pelmenschikov *et al.*, as well as the others mentioned above, tend to overestimate the experimentally measured activation energy in a-SiO_2. Experimental work supports the assertion that the overall activation barrier for siloxane dissociation has an upper bound of $\sim$22 kcal mol^{-1} for bridge dissociation, as shown above. Rimstidt and Barnes have shown that the barrier can be as low as 15 kcal mol^{-1} for an interface of fused quartz and deionized water, at temperatures in the range of 298–573 K.[36] Overall, experimental results reported indicate an activation barrier range of $\sim$14–24 kcal mol^{-1} for the dissolution of a-SiO_2 in water.[5,30,33,36]

Pelmenschikov *et al.* showed the importance of the connectivity of the Si-site to the rest of the lattice *via* the number of bridging oxygens on the activation barrier to dissolution.[34] The other *ab initio* calculations were done on small system sizes that did not account for larger-scale connectivity seen in a-SiO_2 or at its surface and the variability of the ring structure connecting silicate tetrahedra that affect bond angles and reactivities, as seen experimentally.[37,38] In order to incorporate a more robust description of the dissolution of the a-SiO_2 surface, we employed molecular dynamics (MD) computer simulations to investigate the activation barriers for dissolution of a-SiO_2 using H_2O as the primary reagent at a neutral pH. Using a melt-quenched silica substrate surface and multiple starting Q4 sites, we determined the activation barriers obtained from the Q4 site sequentially becoming a Q0 site *via* Q4–Q3–Q2–Q1–Q0 reactions with incoming H_2O. A reactive potential that has been fully tested and accurately reproduces multiple experimental and *ab initio* data for bulk water, nanoconfined water, reactions on silica surfaces and proton transport is used.[39–45] The local structure of the surface defect site is also evaluated to determine the degree to which the barrier is affected.

II. Computational methods

The results obtained in this work have been produced using an all-atom reactive multibody interatomic potential developed to simulate the behavior of bulk water[39] that has been transferred to simulations of nanoconfined water[43–45] and water interacting with an a-SiO_2 surface,[40,41] all with results consistent with either experimental data or *ab initio* calculations. It has also shown proton transport *via* Eigen and Zundel complexes of the Grotthus mechanism with the activation barriers at the O–O spacing in the Zundel complex consistent with *ab initio* calculations and the H_3O^+ ion lifetimes consistent with time-resolved spectroscopies and *ab initio* calculations.[42] The form of the potential involves both two- and three-body terms. The pair term involves a short range repulsion, a coulomb term with diffuse charge terms, and a van der Waals term. The long-range interaction is obtained using Wolf summation[46] with a 10 Å cut-off in a manner previously published.[40,41] A three-body function is further used to allow for the partial covalency and bond directionality of the SiO_2 and H_2O that energetically penalizes a triplet that deviates from the ideal angle, yet allows for deviations from the ideal angle during reactions. Details of the potential have been previously published.[40,41]

Three different vitreous silica surfaces were produced using a melt quench method to form bulk glasses starting from β-cristobalite, followed by formation of the surface systems. Table 1 shows the temperature and number of iterations with a timestep of 1 fs for each glass during the melt-quench to form the amorphous structure.

Variation within the glasses shown in Table 1 was introduced by holding each at 6000 K for a different number of iterations in the first step of the melt quench, creating a different starting liquid.

After the end of the 298 K run, surfaces were created by adding an empty volume of 40 Å in the z dimension and

Table 1 Number of iterations for three samples held at each temperature in melt-quench process

Temperature (K)	Glass1	Glass2	Glass3
6000	30 000	60 000	90 000
4000	100 000	100 000	100 000
3000	100 000	100 000	100 000
2000	100 000	100 000	100 000
1000	40 000	40 000	40 000
298	60 000	60 000	60 000

concurrently freezing the bottom (in z) $\sim$18 Å (1500 atoms) of the glass so as to retain the original bulk-like glass structure in that region and a free surface in the upper z dimension. The final x, y, z dimensions for the system were 35.65 Å, 35.65 Å, and 82.78 Å respectively, with the bottom $\sim$18 Å of frozen silica, $\sim$24 Å of mobile silica, and $\sim$40 Å of space into which water molecules can be added. All subsequent runs were done at 300 K and a timestep of 0.1 fs. Initially, 32 water molecules were added to hydrolyze the surface, potentially allowing for a silanol (SiOH) density of 5.0 SiOH/nm,^{2} which is at the higher end of the experimental average value of $\sim$4–5 SiOH/nm^2 if all of the water reacted. This removed many of the most reactive defect sites caused by the formation of the silica surface. 764 water molecules were then added to the vacuum above the hydroxylated silica surface and allowed to interact with the surface over 400 000 iterations so as to provide a water/silica interface with $\sim$2 nm of water on the silica. Each of the final systems contained 5988 atoms. The dissolution reactions and activation barriers were obtained using calculations of the potential of mean force (PMF) using the H_2O molecule with the correct orientation closest to a particular Q4 Si at the surface in the manner described below. Fifteen (15) initial Q4 sites were randomly selected in the silica surface for the start of the PMF dissolution runs.

III. Potential of mean force

The potential of mean force was calculated by integrating the mean force required to maintain a prescribed radial distance between two atoms in the system for a series of different separation distances. Specifically, the distance between the O of the hydrolyzing H_2O and a target Si with a specific Qi was gradually decreased over the course of the calculation, based upon the initial unconstrained O–Si distance and a final target distance of 1.57 Å. The two criteria for selecting an H_2O to react with the Qi site during the calculation were the distance and location relative to the target siloxane, or bridging, bond (Si–O–Si). A water molecule within approximately 4.5 Å of the site was chosen to allow for the simulations to be completed within a reasonable time and to minimize the possibility that reaction with other water molecules near the Qi site would interfere with the prescribed reactions. The location and orientation of the H_2O relative to the siloxane bond proved to be important. Several preliminary reactions revealed that if the H_2O was not approximately opposite to the target bridge to be hydrolyzed, the H_2O could re-orient around the Si-site tetrahedron during attack and cause the dissociation of an attached silanol on the lower Qi species ($i < 4$), instead of breaking a siloxane bond. In such a case, the i in the Qi label does not change. The re-orientation of this attacking H_2O in such a scenario could occur because the PMF constraint algorithm used here does not control the approach angle of the H_2O but instead allows the molecule to relax into any xyz position based upon the force needed to hold the Si and O at the prescribed radial distances.

The distance between the H_2O oxygen and the Qi Si atom (O–Si pair) was decreased by 0.01 Å during each step of the PMF calculation in a fashion similar to previous work.[42] All other moving atoms in the system were allowed to relax for 10 000 steps (1 ps) before proceeding to the next distance decrement in the PMF calculation. The restoring force that kept the O–Si pair within the small radial range ($\Delta r_{\text{constraint}} < 10^{-5}$ Å) was obtained from the RATTLE algorithm based on the sum of all forces acting on the pair from each other and all other atoms in the system with the 10 Å cut-off during the 10 000 step relaxation. Eventually the distance was reduced to the point that the O reacts with the Qi Si and a siloxane bridge breaks to form a Q($i-1$) site. The reaction occurs when the Qi site becomes pentacoordinated with the attacking H_2O and the four other Si–O bonds, after which a further decrease in separation distance caused a siloxane break and the formation of a non-bridging oxygen (NBO). Upon completion of this force calculation, all moving atoms were allowed to relax over 200 000 steps at 300 K. During this relaxation run, the newly formed NBO was generally protonated by a nearby H_2O to produce an OH^- and a silanol at the location of the NBO. Local charge neutrality was maintained when the reacting H_2O donated a proton to that OH^- (either directly or through proton transport involving nearby H_2O molecules in a Grotthus mechanism; proton transport with this reactive potential has been shown to accurately match *ab initio* calculations of proton transport in bulk water[42]).

After the 200 000 step relaxation run, another H_2O in proximity to the newly formed Q($i-1$) site was chosen and the PMF process was repeated until the Q1 siloxane reacted to form a Q0 $Si(OH)_4$ that was dissolved in solution and no longer connected by any bridges to the silica surface. The mean force required to maintain each specific distance constraint between the reacting species was averaged over the final 5000 iterations of the 10 000 iterations at each distance in the PMF calculation. This force was then integrated over the distance travelled by the attacking H_2O (*i.e.*, the reaction coordinate) and was plotted as the potential of mean force (PMF) *versus* distance to produce a curve for the activation barrier based upon the interatomic potential.

Fifteen Q4 samples used as reaction sites for PMF measurements were located graphically using VMD[47] for the three surfaces available. The samples and respective reactions were identified by capital letter from A to O, and two numbers. The numbers refer to the coordination of the site before and after the reaction; *e.g.* A43 refers to the reaction that converts the sample A Q4 site into a Q3 site. It must by stated explicitly to avoid confusion in this naming scheme that there is no specific sample labeled ''Q''. Any reference using the capital letter Q is

meant to express the type of Si coordination. A reference to Q*ij* refers to a general reaction where a Q*i* site is converted to a Q*j* ($j = (i - 1)$, so Q43 means a Q4 converted to a Q3). The overall reaction from a Q4 to Q0 is labeled Q40 that includes the average of all the dissolution steps going from Q4 to Q0.

IV. Results

The majority of reaction mechanisms observed for each sample followed a similar pattern as the H_2O attacked the Q*i* site. The plane of the tetrahedral non-reacting O–Si–O bridges or silanol groups was observed to flatten out relative to the Q*i* site during the PMF simulation and formed a pentacoordinated distorted trigonal bipyramidal complex with the H_2O during the SN_2-type reaction. The siloxane bridge opposite to the attacking water then dissociated from the Q*i* site and formed an NBO attached to the adjacent Si. This is consistent with other research showing that the back-bond is broken when an H_2O attacks a Q*i* site or when two silicic acid molecules polymerize to form a pyrosilicic acid molecule.[35,48,49] A typical Q43 reaction involving a Q4 site and an H_2O is shown in Fig. 1.

Fig. 1 illustrates the conversion of the Q4 site into a Q3: the H_2O approaches the site, becomes pentacoordinated to the Si atom, and the back bridge siloxane break occurs to form an NBO that is subsequently protonated by nearby system H_2O. Dissociation of the back bridge occurred in almost all of the simulations. A reaction that broke a side siloxane bridge adjacent to the moving water molecule occurred in less than 10% of the simulations, and was observed for only the Q43 reaction in these sites.

Fig. 2a shows the O–Si–O bond angle distribution during the Q43 hydrolysis reaction averaged over the samples, showing the formation of the trigonal bipyramidal five-coordinated Si structure that deviates considerably from the original tetrahedral structure of the initial Si sites (given by the vertical dashed line). The grouping of angles in 2a relate to the instantaneous structure in the snapshot in 2b that shows a 5-coordinated Si during hydrolysis with the angles highlighted. The smaller angles below 100° in 2a come from the angles between the two apical O and the planar oxygen, bounding 90°, with one showing the slightly smaller angle (low 80°'s) and the other showing the concomitant larger angle (high 90°'s). The three planar oxygen fluctuate near 120°, and the angle between the two apical O are near 175°.

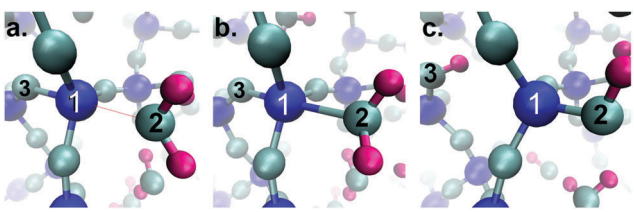

Fig. 1 The C43 reaction, showing the Si Q4 site (1) in (a) and formation of a pentacoordinated complex in response to an attacking H_2O (2) in (b). Dissociation of the back siloxane bridge (3) in (c) to form a Q3 site.

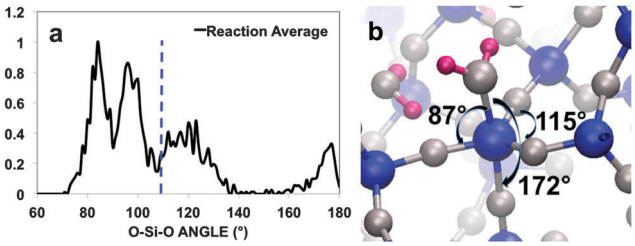

Fig. 2 (a) O–Si–O bond angle distribution during the hydrolysis reaction averaged over the Q43 samples starting from the water oxygen – Si Q4 site distance of 2.3 Å. Dashed line at the tetrahedral angle at 109.5°. (b) Example of an instantaneous structure showing three of the triplets that contribute to the bond angles in (a).

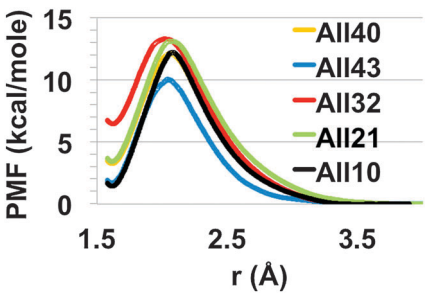

Fig. 3 The average activation barrier curves in each of the four reactions for each sample. The overall average for the four reactions over the 15 samples is labeled as Q40.

Activation barriers were produced for the four reactions of each sample by plotting the integrated mean force *versus* the distance between the Si and the incoming O atom. The PMFs for the fifteen samples were then collected and curves for the average activation barrier summed over the set in each of the reaction steps are shown in Fig. 3. The overall average from all the sites is shown as All40:

Fig. 3 implies that the average barrier for the Q43 reactions was the lowest and the Q32 reactions had the highest activation barriers. The overall activation energy for the formation of an $Si(OH)_4$ Q0 starting from a Q4 is also shown as the average of these average curves. However, the maximum values shown in Fig. 3 and the associated barriers for each reaction obtained from these maxima differ from the average of the specific activation energies calculated from the peak maxima of each of the 15 samples of each Q*ij* curve. These values differ because the top of the barrier for each individual reaction did not occur at the same distance (r) and varied across samples for the same reaction. The effect of the averaging method used for Fig. 3 was to decrease the actual average activation energy plotted here by about 1–1.5 kcal mol^{-1}.

The individual activation barriers for the specific reaction in each sample are shown in Fig. 4a. Calculating the average activation barrier for each Q*ij* from these data gave activation energies and standard deviations for the Q43, Q32, Q21, and Q10 reactions as 10.7 ± 4.1, 14.1 ± 2.9, 14.0 ± 2.5, and 12.6 ± 0.9 kcal mol^{-1}, respectively. The average activation energy from these data for formation of the Q0 from Q4 (All40) is 12.9 ± 1.7 kcal mol^{-1}.

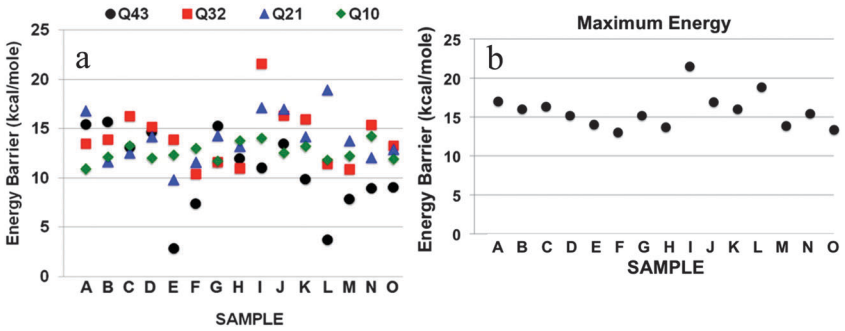

Fig. 4 (a) The activation barriers for each sample in the four Q*ij* reactions, giving an indication that some outliers are present. (b) The maximum energy barrier of each sample, giving the rate-limiting energy barrier of 15.1 kcal mol^{-1}.

However, the rate limiting barrier for the formation of the Q0 from the Q4 would be obtained from the maximum energy barrier for each sample and that is given in Fig. 4b. The average of these maxima gives the activation barrier for dissolution to be 15.1 kcal mol^{-1}. This value fits within the experimental data ranging between 14 and 24 kcal mol^{-1} and fits closely to the experimental data by Rimstidt and Barnes of 15 kcal mol^{-1}.[36]

Another important aspect shown in Fig. 4a is that the Q43 series have a significant number of reactions with low activation barriers. As discussed below, these can be attributed to the distorted structure of these Q4 sites and their connectivity to the rest of the network. If the initial hydroxylation step prior the PMF runs had been longer, more of these low-barrier Q4 sites might have reacted, removing them from selection for the subsequent PMF calculations. In addition, if experimental dissolution begins after initial hydroxylation of silica from the environment in experimental studies, then the experimental dissolution results would start from Q3 sites, not Q4 sites. Most importantly, the simulations show that the rate limiting steps are Q32 and the Q21 sites, each with an activation barrier of ~14.1 kcal mol^{-1}, which fits within lower end of the experimental results.

Fig. 4 indicates that the two lowest barriers in the study occurred in the Q43 reaction for sites E and L at 2.9 and 3.8 kcal mol^{-1} respectively. Site I has the highest barrier in the simulations for the Q32 reaction, at 21.6 kcal mol^{-1}. These sites were investigated graphically to determine whether the cause for variation could be attributed to localized structural effects that produced outliers in the data.

The samples identified as outliers above had local structures and nearby system atoms that altered the reaction mechanism and contributed to barrier differences. The low barriers in the Q43 series showed distorted bond angles associated with the Q4 site that facilitated the rupture of an Si–O bond.

Fig. 5 shows the standard deviation from the tetrahedral angle and the minimum siloxane bond angle (divided by 10 for placement on the same graph) and the resultant energy barrier for the samples. Therefore, each energy barrier has two data points on the graph, as depicted in one case by the dashed horizontal red line. It is clear that a small siloxane bond angle alone is not sufficient to cause a low activation barrier. Rather, the combination of both the small siloxane angle and a large

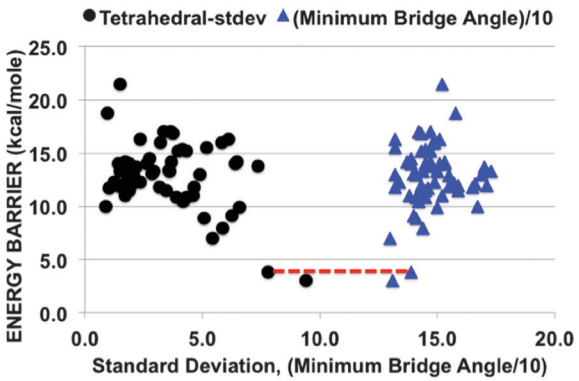

Fig. 5 Standard deviation from the tetrahedral angle and the minimum siloxane bond angle (divided by 10 for placement on the same graph) and the resultant energy barrier for the samples, showing that low energies depend on both structural features. See text.

deviation in the tetrahedral angle provide sufficient distortion in the local structure of the Q4 site to lower the activation barrier to hydrolysis dramatically. Either variation alone is not sufficient.

Reactions for E43 and L43 had the lowest barriers observed in the study. L43 featured the dissociation of a side bridge and the site was a member of a four member ring. The strained angular distribution for the L site included initial tetrahedral angles of 99°, 118°, and 121°. The Si in E43 was a member of two four member rings and had an initial configuration with strained tetrahedral O–Si–O angles of 97° and 128°, as well as one bridge Si–O–Si angle that was 131°. The normal values for these angles would be 109° for the former and 150° for the latter. E43 was abnormal because the H_2O attack caused dissociation of a side bond instead of the back siloxane bond. The site remained energetically unstable because these angles were prevented from assuming equilibrium positions by the lattice. The side-bridge that broke there was on average below 135° for the simulation and thus it was a relatively stable site for proton adsorption.[41,50] This side siloxane acquired a proton concurrent with approach of the reacting H_2O. There is some evidence that the hydroxylated bridge (bridging O with a proton attached, termed BOH[41]) may play some role in encouraging the dissociation of siloxane by decreasing the force necessary for an attacking H_2O to approach the site. Such behavior occurs

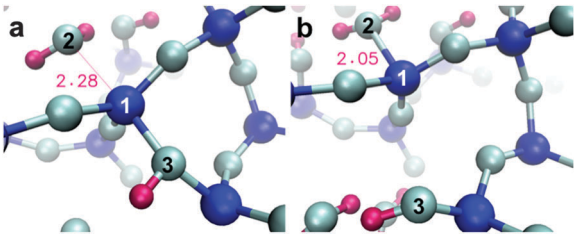

Fig. 6 Two snapshots of the M43 reaction, showing, in (a), the Q4 site (1) approached by the attacking H_2O (2) while an H^+ is adsorbed on the target siloxane bridge (BOH) (3). In (b), as (2) gets closer to (1), the protonated bridge (3) ruptures. Red numbers indicate (2)–(1) distance.

in the M43 reaction, shown in Fig. 6, which shows two moments of the simulation of an H_2O attack on the M Q4 site, where the target siloxane bridge contains a proton, forming a BOH. Sample M contained only one initially strained tetrahedral angle of 122°. The siloxane oxygen (labeled 3 in Fig. 6) is protonated at the start of the simulation with an average bridge angle of 141°. However, this is not a stable bond angle for the proton on this bridge[41] and the proton transfers off and on this oxygen during the early stage of the simulation until the H_2O approaches the site, which gradually lowers this angle, increasing the stability of the BOH, consistent with *ab initio*[50] and MD simulations.[41] When the H_2O – site distance reaches 2.30 Å (O(2)–Si(1)), the proton remains on the O3 bridge for the remainder of the simulations, which helps lower the barrier. Between 2.10 Å and 2.05 Å, the Si(1)–O(3) siloxane bond breaks and reforms, but irreversible siloxane rupture occurs at a bridge angle of 138°, an O(2) to Si(1) distance of 2.05 Å, and a lower barrier of 7.9 kcal mol^{-1}.

The reaction with the highest barrier was I32. The tetrahedral and bridge angles for the site prior to reaction did not show substantial levels of strain. In addition, the site was also lower in the z dimension than other sample sites relative to the ostensible location of the glass–water interface at z = 42 Å in the system. Site I was located at 40.5 Å in z. The reaction for I32 had the highest barrier in the study, and is shown in Fig. 7 with the attacking H_2O at a distance of 2.27 Å from the Si site (the 2–1 separation distance). The hydrogen (3) at the BOH site is 1.46 Å from the attacking O (the 3–2 separation distance), with an O–H–O angle of 160° (the 4–3–2 angle). Of course, these numbers fluctuate during the run. This hydrogen bonding between O(2) and H(3) caused an increase in the restorative forces required to bring the attacking O towards the equilibrium distance to the Si

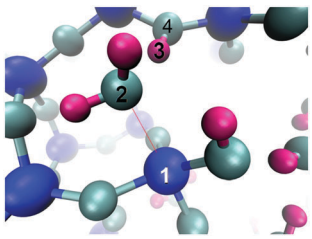

Fig. 7 The I32 reaction. The Q3 site (1) is approached by an H_2O (2) that is hydrogen bonded to a nearby BOH (3).

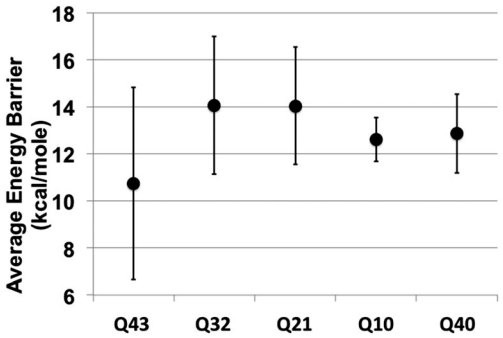

Fig. 8 The average energy barriers for each Q*i* reaction for all of the samples.

site in the PMF calculations, evidenced by a significantly higher slope in the curve and higher barrier for the I32 barrier (curve not shown here).

The differences in the outlier samples discussed above indicate that these factors of the pre-reaction localized strain, the presence or lack of lattice constraints, and the interactions with adjacent atoms near, but not on, the reaction site could play a role in producing an unusually low or high barrier for the rupture of a siloxane bridge. The average value for the activation barrier is shown in Fig. 8, along with error bars that represent the variation across the 15 samples in each reaction. The standard deviation for the barrier decreases in the later stages of dissolution, when the coordination number of the defect is lowered, as indicated by the broad distribution in the Q43 and the narrow distribution in the Q10 reactions of Fig. 8. Q40 gives these data averaged over all reactions starting from the Q4 down to the Q0.

V. Discussion

The data obtained during the course of this study indicates that the rate-limiting steps obtained in the simulations are the Q32 and Q21 reactions, each with an average of ~14 kcal mol^{-1}. As presented above, the Q43 reaction has the lowest average activation barrier and the largest number of very low individual barriers because of the increased number of strained siloxane bonds at these Q4 sites prior to the reaction. Had the initial hydroxylation continued for longer times, these lower barrier sites might have been removed prior to the PMF calculations. This is important in that experimental data are taken after the silica has already been exposed to the environment and complete hydroxylation would have occurred, removing these low-barrier, or more easily reactive, Q4 sites, so that the dissolution reactions would have started from the Q3 species. In any case, the result showing the rate-limiting barrier using the maximum energy barrier for each sample (Fig. 4b) of 15.1 kcal mol^{-1} in the simulations is quite reasonable in comparison to the experimental data that obtain activation barriers for dissolution of a-SiO_2 in water in the range of ~14–24 kcal mol^{-1}.[5,33,36] The energy barrier reported here is lower than that observed in a number of previous computational studies that obtained

barriers in the range of 17.7–38.7 kcal mol^{-1} depending upon reactant molecule, form of silica, and number of additional waters: Xiao and Lasaga (18.9–29 kcal mol^{-1}),[20] Pelmenschikov *et al.* (20–29 kcal mol^{-1}),[5] Walsh *et al.* (24 kcal mol^{-1}),[31] Del Bene *et al.* (30 kcal mol^{-1}),[32] Criscenti *et al.* (17.7–28.4 kcal mol^{-1}),[7] Wallace *et al.* (38.7 kcal mol^{-1}).[30] Those previous calculations used smaller system sizes and most investigated a cluster structure meant to mimic crystalline silica and not a-SiO_2. Several studies had a limited number of H_2O molecules to participate in the reaction at the surface that may have played a role in producing an elevated barrier. I32 was the only reaction where the activation barrier was above 20 kcal mol^{-1} in this study. The observations discussed above for the I32 reaction suggests that H-bonding to nearby NBO or hydrogen on bridging oxygen (BOH) affected the reaction mechanism. The site was located in surface contours below the average surface and the barrier appears to be elevated due to attractive forces to nearby surface lattice sites that are lateral or slightly higher in *z* dimension that would not be present at the outermost surface where the reactant is less restricted by the local structure. In addition, the lower location of the site relative to the surface inhibited reaction with additional unconstrained H_2O that could have contributed to supplying protons to the siloxane bonds about to rupture, thus raising the barrier.

The magnitude of the differences in activation energy for the different Q*i* species appears to be mediated by the degree of strain or the available H_2O pathways at the reaction site. The approach of the attacking H_2O to the site in an SN_2-type reaction causes the three adjacent oxygen bridges or silanol sites to enter into a flat plane as a distorted pentacoordinated trigonal bipyramid complex is formed and the back siloxane dissociates. The flattening of the plane requires a certain amount of energy because the angles of the pentacoordinated complex are by definition non-equilibrium, relative to tetrahedral SiO_2 units. The tetrahedral angle of the O–Si–O atoms in the flat plane for the activated complex increases from approximately 109° to 120°. The O–Si–O angle between the target bridge and the Si–O members of the plane must decrease from 109° to ~90°. The Q4 site contains three siloxane bonds that may contribute to resistance in the flattening of the plane (the lattice constraint), and the site should intuitively have the highest activation barrier. However, the Q4 sites randomly selected here showed the largest propensity to have initially strained angles. These angles require smaller energetic contributions before a pentacoordinated complex is formed. The simplified explanation for the low Q4 barrier is consistent with results showing a lower barrier for the Q1 site as well. The Q1 site contains only one bridge and three silanol groups; the silanol groups assume equilibrium angles around the Q1 and show no strain. The approach of the attacking H_2O opposite the sole siloxane bridge requires the rearrangement of only silanol groups to form the flattened plane of the pentacoordinated complex. Less energy is required to achieve the non-equilibrium angles in the activated complex because the silanols do not have the same lattice resistance to attacking H_2O that the siloxane bonds would have. The Q1 defect site showed almost no strained bond angles in any of the samples, and the Q3 and Q2 sites investigated showed some strain but it was considerably less than the strain presented by the Q4 site.

The surface Si sites with a lower number of bridging oxygen will experience less resistance to strain during the reaction because these sites are freer to relax (less lattice constraint). Ignoring the presence of either H_3O^+ or OH^- ions as the reactants and assuming only H_2O as the reactant, an ideal reaction would involve an H_2O becoming coordinated to the Si site *via* the pentacoordinated Si trigonal bipyramid, rupture of the bridge with possible simultaneous transport of a proton from the attacking or a nearby H_2O to the NBO, and the formation of silanol groups.

VI. Conclusion

Molecular dynamics simulations were used to determine the activation barriers to the dissolution of the amorphous SiO_2 surface in the presence of a 2 nm overlayer of water. The potential of mean force calculations of the reactions of water molecules with multiple starting Q4 sites to eventually form the dissolved Q0 site were used to determine the barriers. Activation barriers for each step in the dissolution process, from the Q4 to Q3 to Q2 to Q1 to Q0 were obtained for 15 different starting Q4 sites. Relaxation runs between each reaction step enabled redistribution of the 2 nm water layer in response to the new Q*i* site configuration. The rate-limiting steps observed in the simulations were in the Q32 reactions (a Q3 site changing to a Q2 site) and Q21 reactions, with an average barrier of 14 kcal mol^{-1}. The rate-limiting energy barrier obtained from the maximum barrier from each sample was 15.1 kcal mol^{-1}. This result is within the lower end of the experimental data, which varies from 18–24 kcal mol^{-1}, while various *ab initio* calculations using small cluster models obtain values that vary from 18–39 kcal mol^{-1}.

The steric restrictions in each defect site produced different degrees of angular strain and limitations on proton transport to the reaction site in the system. The low barriers in the Q43 reaction (average 10.7 kcal mol^{-1}) were attributed to pre-reaction angular strain in these sites that enable easier rupture of these strained siloxane bonds in response to the incoming H_2O molecule. Had hydroxylation of the surface been carried out for a longer time in the simulations, some of these distorted Q4 sites may have been hydrolyzed to Q3 sites prior to the PMF calculations, removing some of the sites with the lowest Q43 barriers observed here. More importantly, the presence of such strained Q4 sites would not be present in dissolution experiments where all such sites would have been reacted and the dissolution barriers would have been representative of reactions starting from Q3 sites. The Q21 reaction had a barrier (14.0 kcal mol^{-1}) similar to the Q32 barrier. The low barrier in the Q10 (12.6 kcal mol^{-1}) was attributed to lower resistance by the three silanols on the Q1 site to formation of the pentacoordinated trigonal bipyramid complex that acts as the intermediate state in the reaction.

The highest barrier ($\sim$22 kcal mol^{-1}) occurred at Si sites that were in slightly concave surface contours below the outermost surface, allowing the incoming reacting H_2O molecule to interact with nearby atoms at z dimensions slightly above the Si. These interactions provided forces opposed to the interaction with the reactant Si site, increasing the effective restoring forces in the PMF calculations and raising the barrier.

References

1 T. Hiemstra and W. H. Riemsdijk, *J. Colloid Interface Sci.*, 1990, **136**, 132–150.
2 S. Nangia and B. J. Garrison, *J. Phys. Chem. C*, 2010, **114**, 2267–2272.
3 W. H. Casey and G. Sposito, *Geochim. Cosmochim. Acta*, 1992, **56**, 3825–3830.
4 S. Nangia and B. J. Garrison, *J. Phys. Chem. A*, 2008, **112**, 2027–2033.
5 A. G. Pelmenschikov, J. Leszczynski and L. G. M. Pettersson, *J. Phys. Chem. A*, 2001, **105**, 9528–9532.
6 W. H. Casey, A. C. Lasaga and G. V. Gibbs, *Geochim. Cosmochim. Acta*, 1990, **54**, 3369–3378.
7 L. J. Criscenti, J. D. Kubicki and S. L. Brantley, *J. Phys. Chem. A*, 2006, **110**, 198–206.
8 Z. M. Du and N. H. de Leeuw, *Dalton Trans.*, 2006, 2623–2634.
9 A. C. Lasaga, in *Chemical Weathering Rates of Silicate Minerals*, ed. A. F. White and S. L. Brantley, Mineralogical Society of America, Washington, D.C., 1995, vol. 31, pp. 23–86.
10 A. J. Gratz, S. Manne and P. K. Hansma, *Science*, 1991, **251**, 1343–1346.
11 P. Dove and D. Crerar, *Geochim. Cosmochim. Acta*, 1990, **54**, 955–969.
12 T. A. Michalske and B. C. Bunker, *J. Appl. Phys.*, 1984, **56**, 2686–2693.
13 T. A. Michalske and E. Fuller, *J. Am. Ceram. Soc.*, 1985, **68**, 586–590.
14 S. Wiederhorn, E. Fuller and R. Thomson, *Met. Sci.*, 1980, 450–458.
15 S. Ito and M. Tomozawa, *J. Am. Ceram. Soc.*, 1982, **65**, 368–371.
16 T. Michalske and S. Freiman, *Nature*, 1982, **295**, 511–512.
17 S. Wiederhorn, *Commun. Am. Ceram. Soc.*, 1982, C-202–C-203.
18 Y. Bando, S. Ito and M. Tomozawa, *J. Am. Ceram. Soc.*, 1984, C36–C37.
19 S. M. Wiederhorn, T. Fett, G. Rizzi, S. Fünfschilling, M. J. Hoffmann and J.-P. Guin, *J. Am. Ceram. Soc.*, 2011, **94**, s196–s203.
20 Y. Xiao and A. C. Lasaga, *Geochim. Cosmochim. Acta*, 1994, **58**, 5379–5400.
21 J. D. Kubicki, Y. Xiao and A. C. Lasaga, *Geochim. Cosmochim. Acta*, 1993, **57**, 3847–3853.
22 *Chemical Weathering Rates of Silicate Minerals*, ed. A. F. White and S. L. Brantley, Mineralogical Society of America, Washington, D.C., 1995.
23 S. Wiederhorn, *J. Am. Ceram. Soc.*, 1971, **55**, 81–85.
24 S. M. Wiederhorn, H. Johnson, A. M. Diness and A. H. Heuer, *J. Am. Ceram. Soc.*, 1974, **57**, 336–341.
25 P. Frugier, S. Gin, Y. Miner, T. Chave, B. Bonin, N. Godon, J.-E. Lartigue, P. Jolliver, A. Ayral, L. De Windt and G. Sanrarini, *J. Nucl. Mater.*, 2008, **380**, 8–21.
26 D. Strachan and T. L. Croak, *J. Non-Cryst. Solids*, 2000, **272**, 22–33.
27 C. Cailleteau, F. Angeli, F. Devreux, S. Gin, J. Jestin, P. Jollivet and O. Spalla, *Nat. Mater.*, 2008, **7**, 978–983.
28 R. Conradt, *J. Am. Ceram. Soc.*, 2008, **91**, 728–735.
29 S. Nangia and B. J. Garrison, *Theor. Chem. Acc.*, 2010, **127**, 271–284.
30 A. F. Wallace, G. V. Gibbs and P. M. Dove, *J. Phys. Chem. A*, 2010, **114**, 2534–2542.
31 T. R. Walsh, M. Wilson and A. P. Sutton, *J. Chem. Phys.*, 2000, **113**, 9191–9200.
32 J. E. Del Bene, K. Runge and R. J. Bartlett, *Comput. Mater. Sci.*, 2003, **27**, 102–108.
33 J. P. Icenhower and P. M. Dove, *Geochim. Cosmochim. Acta*, 2000, **64**, 4193–4203.
34 A. Pelmenschikov, H. Strandh, L. G. M. Pettersson and J. Leszczynski, *J. Phys. Chem. B*, 2000, **104**, 5779–5783.
35 R. K. Iler, *The Chemistry of Silica*, John Wiley and Sons, New York, 1979.
36 J. D. Rimstidt and H. L. Barnes, *Geochim. Cosmochim. Acta*, 1980, **44**, 1683–1699.
37 C. J. Brinker, R. K. Brow, D. R. Tallant and R. J. Kirkpatrick, *J. Non-Cryst. Solids*, 1990, **120**, 26–33.
38 B. C. Bunker, D. M. Haaland, T. A. Michalske and W. L. Smith, *Surf. Sci.*, 1989, **222**, 95–118.
39 T. S. Mahadevan and S. H. Garofalini, *J. Phys. Chem. B*, 2007, **111**, 8919–8927.
40 T. S. Mahadevan and S. H. Garofalini, *J. Phys. Chem. C*, 2008, **112**, 1507–1515.
41 G. K. Lockwood and S. H. Garofalini, *J. Chem. Phys.*, 2009, **131**, 074703.
42 G. K. Lockwood and S. H. Garofalini, *J. Phys. Chem. B*, 2013, **117**, 4089–4097.
43 S. Xu, G. C. Simmons, T. S. Mahadevan, G. W. Scherer, S. H. Garofalini and C. Pacheco, *Langmuir*, 2009, **25**, 5084–5090.
44 S. Xu, G. W. Scherer, T. S. Mahadevan and S. H. Garofalini, *Langmuir*, 2009, **25**, 5076–5083.
45 S. H. Garofalini, T. S. Mahadevan, S. Xu and G. W. Scherer, *ChemPhysChem*, 2008, **9**, 1997–2001.
46 D. Wolf, P. Keblinski, S. R. Phillpot and J. Eggebrecht, *J. Chem. Phys.*, 1999, **110**, 8254–8282.
47 W. Humphrey, A. Dalke and K. Schulten, *J. Mol. Graphics*, 1996, **14**, 33–38.
48 B. F. Feuston and S. H. Garofalini, *Chem. Phys. Lett.*, 1990, **170**, 264–270.
49 G. Martin and S. H. Garofalini, *J. Non-Cryst. Solids*, 1994, **171**, 68–79.
50 K. Vanheusden, P. P. Korambath, H. A. Kurtz, S. P. Karna, D. M. Fleetwood, W. M. Shedd and R. D. Pugh, *IEEE Trans. Nucl. Sci.*, 1999, **46**, 1562–1567.

PCCP

CORRECTION

Cite this: *Phys. Chem. Chem. Phys.*, 2014, **16**, 25649

Correction: Reactive simulations of the activation barrier to dissolution of amorphous silica in water

Michael Kagan, Glenn K. Lockwood and Stephen H. Garofalini*

DOI: 10.1039/c4cp90161d

www.rsc.org/pccp

Correction for 'Reactive simulations of the activation barrier to dissolution of amorphous silica in water' by Michael Kagan *et al., Phys. Chem. Chem. Phys.*, 2014, **16**, 9294–9301.

On page 9300, in the last sentence of the first paragraph of the Conclusions, the first data range is incorrectly shown as 18–24 kcal mol^{-1}, instead of 14–24 kcal mol^{-1}. The sentence should therefore read as follows:

This result is within the lower end of the experimental data, which varies from 14–24 kcal mol^{-1}, while various *ab initio* calculations using small cluster models obtain values that vary from 18–39 kcal mol^{-1}.

The Royal Society of Chemistry apologises for these errors and any consequent inconvenience to authors and readers.

Interfacial Molecular Science Laboratory, Department of Materials Science and Engineering, Rutgers University, Piscataway, NJ, 08854, USA. E-mail: shg@rutgers.edu